

Astrophysical and experimental implications from the magnetorotational instability of toroidal fields

G. Rüdiger,^{1,2★} M. Gellert,¹ M. Schultz,¹ R. Hollerbach^{3,4} and F. Stefani²

¹Leibniz-Institut für Astrophysik Potsdam, An der Sternwarte 16, D-14482 Potsdam, Germany

²Helmholtz-Zentrum Dresden-Rossendorf, POB 51 01 19, D-01314 Dresden, Germany

³Department of Applied Mathematics, University of Leeds, Woodhouse Lane, Leeds LS2 9JT, UK

⁴ETH Zürich, Institut für Geophysik, Sonneggstr 5, CH-8092 Zürich, Switzerland

Accepted 2013 November 7. Received 2013 October 31; in original form 2013 March 21

ABSTRACT

The interaction of differential rotation and toroidal fields that are current-free in the gap between two corotating axially unbounded cylinders is considered. It is shown that non-axisymmetric perturbations are unstable if the rotation rate and Alfvén frequency of the field are of the same order, almost independent of the magnetic Prandtl number Pm . For the very steep rotation law $\Omega \propto R^{-2}$ (the Rayleigh limit) and for small Pm , the threshold values of rotation and field for this azimuthal magnetorotational instability (AMRI) scale with the ordinary Reynolds number and the Hartmann number, respectively. A laboratory experiment with liquid metals like sodium or gallium in a Taylor–Couette container has been designed on the basis of this finding. For fluids with more flat rotation laws, the Reynolds number and the Hartmann number are no longer typical quantities for the instability. For the weakly non-linear system, the numerical values of the kinetic energy and the magnetic energy are derived for magnetic Prandtl numbers ≤ 1 . We find that the magnetic energy grows monotonically with the magnetic Reynolds number Rm , while the kinetic energy grows with Rm/\sqrt{Pm} . The resulting turbulent Schmidt number, as the ratio of the ‘eddy’ viscosity and the diffusion coefficient of a passive scalar (such as lithium), is of the order of 20 for $Pm = 1$, but for small Pm it drops to the order of unity. Hence, in a stellar core with fossil fields and steep rotation law, the transport of angular momentum by AMRI is always accompanied by an intense mixing of the plasma, until the rotation becomes rigid.

Key words: instabilities – MHD – stars: interiors – stars: magnetic field.

1 INTRODUCTION

A hydrodynamically stable rotation law may become unstable under the presence of a sufficiently strong uniform axial field. For this so-called magnetorotational instability (MRI), the axial field provides the catalyst which makes the rotation law unstable without any modification of the uniform field (Velikhov 1959). Of course, by this mechanism, a protoplanetary disc with a Keplerian rotation law should also become unstable if it is not too cold or – (almost) equivalently – if the field is strong enough. For an estimation of the critical magnetic field strength, it is enough to use the condition $S \gtrsim 1$, where the Lundquist number $S = B_z H / \sqrt{\mu_0 \rho} \eta$, with B_z the amplitude of the axial field, H the semi-thickness of the disc and η the microscopic magnetic diffusivity. Plotted in the S – Rm plane, with $Rm = \Omega H^2 / \eta$ as the magnetic Reynolds number, and for small magnetic Prandtl number

$$Pm = \nu / \eta, \quad (1)$$

the viscosity hardly influences the instability map. At a distance of 1 au from a central mass with $1 M_\odot$, the disc thickness is about 3 per cent, the density ρ of the gas $10^{-10} \text{ g cm}^{-3}$ and $\eta \simeq 4 \times 10^{15} \text{ cm}^2 \text{ s}^{-1}$ (because of the low temperature of the gas). Hence, the surprisingly high value of 0.1 G is obtained for the minimum B_z .

In order to excite non-axisymmetric MRI modes, one needs even higher magnetic fields. Kitchatinov & Rüdiger (2010) showed in a linear theory that non-axisymmetric modes only arise if $\Omega_A \gtrsim 0.05 \Omega$, with the Alfvén frequency $\Omega_A = B_z / \sqrt{\mu_0 \rho} H$. For $\Omega = 2 \times 10^{-7} \text{ s}^{-1}$ at 1 au, this condition is fulfilled for $B_z \gtrsim 0.3 \text{ G}$. Such strong fields at this distance cannot be due to a stellar dipole field in the centre. On the other hand, one should mention that the fossil magnetic fields found in meteorites are of just this order. One solution of this dilemma is to consider toroidal fields, which by the stretching action of differential rotation may often exceed the values of the poloidal field. For protoplanetary discs, however, the magnetic Reynolds number Rm only reaches values of about 50, so that the resulting toroidal field does *not* dominate the original B_z .

★E-mail: gruediger@aip.de

The same is true for galaxies when the interstellar turbulence is driven by SN explosions. The resulting magnetic Reynolds number is then also of the order of 10–100, so that the induced toroidal field does not dominate the poloidal one – as observed.

A very different situation holds for the radiative cores of rotating stars. Due to the high conductivity of the hot plasma, the magnetic Reynolds number is so large that even very slight differential rotation will produce toroidal fields which clearly dominate the fossil poloidal fields. It should then be sufficient to consider the stability of only the strong toroidal field under the presence of differential rotation. In the present paper, we shall always apply a rotation law close to the profile of uniform specific angular momentum, i.e. $\Omega \propto R^{-2}$. This rather steep profile is just beyond the regime of hydrodynamic centrifugal instability, also in spherical systems (see Rüdiger & Kitchatinov 1996).

There are basic stability conditions in cylindrical geometry. A flow is stable against axisymmetric perturbations if

$$\frac{d}{dR} (R^2 \Omega)^2 > \frac{R^4}{\mu_0 \rho} \frac{d}{dR} \left(\frac{B_\phi^2}{R^2} \right) \quad (2)$$

(Michael 1954). This condition turns into the well-known Rayleigh criterion for both $B_\phi = 0$ and $B_\phi \propto R$. The latter case means that an axial uniform electric current does not suppress Taylor vortices, which are due to too steep rotation profiles. Hence, rotation laws which are steeper than $\Omega \propto R^{-2}$ will always excite axisymmetric rolls, even under the presence of very strong toroidal fields with $B_\phi \propto R$. On the other hand, any unstable Ω profiles can be stabilized with a toroidal field of sufficiently large amplitude and suitable geometry.

If non-axisymmetric modes are considered, then the necessary and sufficient condition for stability becomes

$$\frac{d}{dR} (R B_\phi^2) < 0 \quad (3)$$

(Tayler 1957, 1973; Vandakurov 1972), at least in the absence of rotation. The fully general formulation including rotation is not known. Two questions immediately arise: (i) is the field corresponding to a uniform current ($B_\phi \propto R$) really unstable? and (ii) does the current-free field $B_\phi \sim R^{-1}$ become unstable under the presence of (differential) rotation? Both questions can be answered. In the first case, the resulting instability is called the Tayler instability (TI), and in the second case, where fields and rotation profiles that would each be stable on their own interact to yield instability, the result is called the azimuthal magnetorotational instability (AMRI). Whereas the energy for the TI comes from the electric current, the energy source for AMRI is entirely from the differential rotation, and AMRI can only saturate at the expense of the rotational shear by producing high values of ‘eddy’ viscosity. This could therefore justify the high values of ‘artificial’ viscosity which Eggenberger, Montalbán & Miglio (2012) introduced to explain the slow rotation of the stellar cores after the collapse towards their red giant stage.

The interaction of flow and field has already been considered by Chandrasekhar (1956) who proved that for ideal media the system $U_\phi(R)$ and $B_\phi(R)$ is stable for $U_\phi(R) = B_\phi(R)$. Indeed, the current-free (AMRI) field $B_\phi \propto R^{-1}$ subject to the rotation with $\Omega \propto R^{-2}$ (Rayleigh limit) belongs to this class. Instability is thus only possible for $\Omega \neq \Omega_A$ with the Alfvén frequency $\Omega_A = B_\phi / \sqrt{\mu_0 \rho R^2}$. Fig. 1 (left-hand panel) as a result of numerical calculations indeed shows the realization of this finding for finite diffusivities. The lower branches for $\text{Pm} = 1$ and 10 are very close to that limit. For very small Pm it is the upper branch which approaches the Chandrasekhar line $\Omega = \Omega_A$ from below.

2 THE DISPERSION RELATION FOR $\Omega \propto R^{-2}$

It is possible to demonstrate the mechanism which leads to AMRI with a simple dispersion relation for the stability of non-axisymmetric perturbations in the form $\exp(\omega t + i(k_z z + k_R R + m\phi))$ with the real part $\Re(\omega)$ as the growth rate. It is enough to apply the case with $\text{Pm} \rightarrow 0$ and $\Omega \propto 1/R^2$ (the Rayleigh limit) together with $B_\phi \propto R^{-1}$ to the expressions given by Kirillov, Stefani & Fukumoto (2012) for non-axisymmetric perturbations. The resulting dispersion relation is of second order, i.e.

$$\text{Re}^2 \hat{\omega}^2 + \text{Re} (a_3 + ib_3) \hat{\omega} + a_4 + ib_4 = 0. \quad (4)$$

Here we have used the quantity $\hat{\omega} = \omega/\Omega$ as the growth rate in units of the angular velocity of rotation and the Reynolds number $\text{Re} = \Omega/\nu k^2$. The imaginary part of $\hat{\omega}$ describes an azimuthal drift $\hat{\omega}_{\text{dr}}$ of the non-axisymmetric pattern (see below). The coefficients in (4) are

$$\begin{aligned} a_3 &= 2(1 + (2 + m^* \text{Ha}^{*2})), & b_3 &= 2m^* \text{Re}^*, \\ a_4 &= 1 + (4 + 2m^{*2}) \text{Ha}^{*2} + m^{*4} \text{Ha}^{*4} - m^{*2} \text{Re}^{*2}, \\ b_4 &= 2\text{Re}^* m^* (1 + m^{*2} \text{Ha}^{*2}), \end{aligned} \quad (5)$$

with the abbreviations

$$\text{Re}^* = \alpha \text{Re}, \quad \text{Ha}^* = \frac{\alpha}{kR} \text{Ha}, \quad m^* = \frac{m}{\alpha}, \quad (6)$$

where $\alpha = k_z/k$ and $\text{Ha} = B_\phi / (k \sqrt{\mu_0 \rho \nu \eta})$.

The formal solution of (4) for marginal instability leads to the following two conditions:

$$\hat{\omega}_{\text{dr}} = -\frac{b_4}{\text{Re} a_3}, \quad a_3(a_3 a_4 + b_3 b_4) = b_4^2. \quad (7)$$

The first of these relations gives the negative drift rate in units of the basic rotation, i.e.

$$\frac{\omega_{\text{dr}}}{\Omega} = -\frac{m(1 + m^{*2} \text{Ha}^{*2})}{1 + (2 + m^{*2}) \text{Ha}^{*2}}. \quad (8)$$

The observable drift in the laboratory system, $d\phi/dt = -\omega_{\text{dr}}/m$, is thus positive (in the rotation direction) and with $d\phi/dt/\Omega \leq 1$. This value is reduced by medium Hartmann numbers, but it is independent of the magnetic field for large Hartmann numbers. Note the absence of the magnetic Prandtl number in the relation (8). For small Pm , the drift values (and also the axial wavenumbers) do not depend on the actual values of Pm (see Fig. 1). The phase speed $d\phi/dt$ is also independent of the sign of the mode number m .

The second condition in (7) leads to

$$\text{Re}^* \simeq \frac{m^{*3} \text{Ha}^{*2}}{2}, \quad (9)$$

the latter relation holding for strong fields. Axisymmetric solutions do not exist. It is also clear that the mode with $m = 1$ is most easily excited so that

$$\frac{\text{Ha}^2}{\text{Re}} \simeq 2k_z^2 R^2, \quad (10)$$

again valid for large Ha . The influence of the axial wavenumber on the excitation condition is rather strong. Solutions with a large axial wavenumber – representing oblate cells – require much slower rotation to be excited than round cells. For the Elsasser number $\Lambda = B_\phi^2 / \mu_0 \rho \eta \Omega$ one obtains $\Lambda \simeq 2(k_z R)^2$, where the influence of both the microscopic viscosity and the radial wavenumber completely disappears. Note that the normalized wavenumber $k_z R$ is of the order of unity for spheres or axially unbounded cylinders but is

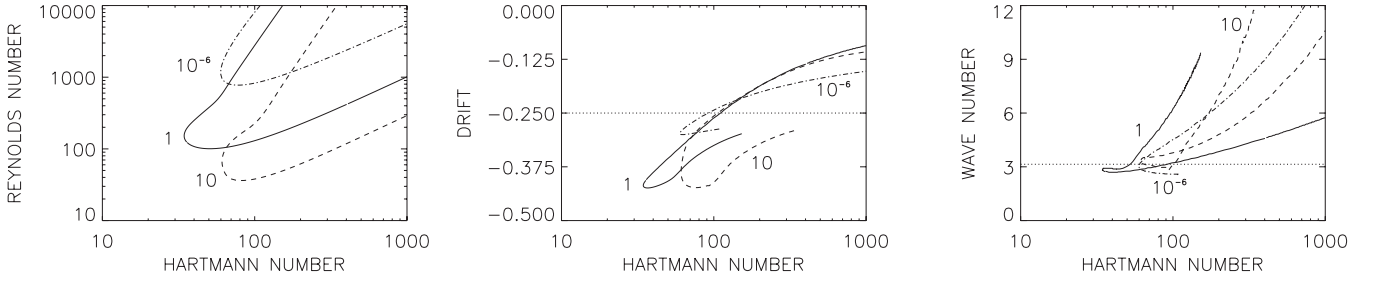


Figure 1. The AMRI at the Rayleigh limit ($R^2\Omega = \text{constant}$, i.e. $\mu_\Omega = 0.25$) for the magnetic Prandtl numbers $\text{Pm} = 10^{-6}$, 1 and 10. Left-hand panel: the instability map; middle panel: the azimuthal drift of the solutions normalized with Ω_{in} ; right-hand panel: the axial wavenumber k multiplied with the gap width D . The Reynolds numbers, the drift values and the wavenumbers for $\text{Pm} < 10^{-4}$ cannot be distinguished from the values at the given lines for $\text{Pm} = 10^{-6}$.

much larger for thin discs. Another interesting reformulation of this relation is

$$\frac{\Omega_A^2}{\Omega^2} \simeq \frac{2k_z^2 R^2}{\text{Rm}} \quad (11)$$

with $\text{Rm} = \text{Pm Re}$. It is thus clear that for large enough η , i.e. for sufficiently low electric conductivity, the ratio (11) may exceed unity, which is not the case for $\text{Pm} = 1$ (see Fig. 1, left-hand panel). Hence, for a small magnetic Prandtl number AMRI exists in the strong-field limit ($\Omega_A > \Omega$), while the opposite is true ($\Omega_A < \Omega$) for $\text{Pm} \geq 1$. Equation (11) with $k_z \simeq \pi/H$ and with the above given disc parameters leads to a critical magnetic field of $B_\phi \simeq 3R/H \simeq 100$ G, the latter for a thin disc with $H/R \simeq 0.03$. One needs about 10^{-2} G poloidal field to induce toroidal fields with 100 G in such discs.

For the inner radiative zones of hot giants, the relation (11) turns into $\Omega_A^2 \simeq 10\eta\Omega$ which with $\rho \simeq 10 \text{ g cm}^{-3}$, $\eta \simeq 10^2 \text{ cm}^2 \text{ s}^{-1}$ and $\Omega \simeq 10^{-5} \text{ s}^{-1}$ provides about 1 G as the threshold value of the toroidal field.

3 A HYDROMAGNETIC TAYLOR-COUETTE PROBLEM

With a view on the experimental demonstration of AMRI, we consider a Taylor–Couette set-up with two corotating cylinders of nearly perfectly conducting material. The cylinders confine an incompressible, conducting fluid under the presence of a toroidal magnetic field. It is clear that the radial profiles of the rotating flow and the field between the cylinders are

$$U_\phi = R\Omega = a_\Omega R + \frac{b_\Omega}{R}, \quad B_\phi = a_B R + \frac{b_B}{R}. \quad (12)$$

Let the ratio of the rotation rates of the cylinders be $\mu_\Omega = \Omega_{\text{out}}/\Omega_{\text{in}}$ and a similar expression for the field amplitudes, i.e.

$$\mu_B = \frac{B_{\text{out}}}{B_{\text{in}}}. \quad (13)$$

The ratio of the cylinder radii is $r_{\text{in}} = R_{\text{in}}/R_{\text{out}}$, where we will fix $r_{\text{in}} = 0.5$. For such a container $\mu_\Omega = 0.25$ describes the Rayleigh limit for which $R^2\Omega \simeq \text{constant}$ ($a_\Omega = 0$ in equation (12)), while $\mu_\Omega = 0.5$ describes the quasi-galactic rotation law $U_\phi \simeq \text{constant}$. These two rotation laws form the extremes which will be considered here in detail. As they behave rather differently, the solutions for the rotation laws between them (e.g. the Kepler rotation law) should be more complex and might even depend on the boundary conditions. As a special choice for a laboratory experiment also a rotation law with $\mu_\Omega = 0.26$ has been considered which is hydrodynamically stable but close enough to the Rayleigh limit to become unstable with rather weak magnetic fields and slow basic rotation (see below).

The magnetic profile in (12) also contains two extrema. With $b_B = 0$ the toroidal field is due to a homogeneous current inside the fluid. For $r_{\text{in}} = 0.5$ the corresponding value is $\mu_B = 2$. Such fields are unstable according to the criterion (3) against non-axisymmetric perturbations. The existence of this kink-type ‘Taylor’ instability has recently been shown in the laboratory (Rüdiger et al. 2012; Seilmayer et al. 2012).

The equations and boundary conditions are given by Rüdiger et al. (2007) and will not be repeated here. The cylinders, which are unbounded in the axial direction, are imagined to be made of a perfectly conducting material. The AMRI in the container with $r_{\text{in}} = 0.5$ appears for $\mu_B = 0.5$. The electric current only flows within the inner cylinder.

The main parameters of the theory are the Reynolds number and the Hartmann number defined by

$$\text{Re} = \frac{\Omega_{\text{in}} D^2}{\nu}, \quad \text{Ha} = \frac{B_{\text{in}} D}{\sqrt{\mu_0 \rho \nu \eta}}, \quad (14)$$

with $D = R_{\text{out}} - R_{\text{in}}$ and the corresponding magnetic Reynolds number $\text{Rm} = \text{Pm Re}$ and the Lundquist number $S = \sqrt{\text{Pm}} \text{Ha}$.

For the rotation law with $\mu_\Omega = 0.25$ (the Rayleigh limit), the plots in Fig. 1 demonstrate the characteristic values of the solutions. The critical Reynolds numbers (left-hand panel), drift rates (middle panel) and wavenumbers (right-hand panel) are given for the magnetic Prandtl numbers 10^{-6} , 1 and 10, which differ by many orders of magnitude. The differences of the characteristic values given in Fig. 1, however, remain very small. In terms of the Reynolds number, the AMRI at the Rayleigh limit can be more easily excited for $\text{Pm} = 1$ than for $\text{Pm} \rightarrow 0$, but the effect is only weak compared with the variation of the magnetic Prandtl number. Obviously, the AMRI close to the Rayleigh limit scales for very small Pm with the Reynolds number Re and the Hartmann number Ha (Hollerbach, Teeluck & Rüdiger 2010). As an immediate consequence, the existence of the AMRI can be proven by laboratory experiments with liquid metals with their very low values of Pm – just as the helical MRI (Stefani et al. 2009), but in strong contrast to the standard MRI which is much harder to achieve (Rüdiger & Hollerbach 2004). The results obtained with materials with low Pm are also representative of materials with Pm of the order of unity. Typical values for such possible experiments are $\text{Re} \simeq 1000$ and $\text{Ha} \simeq 100$ (see below).

For $\text{Pm} \gtrsim 1$ the mentioned scaling changes, but we do not discuss these cases here in more detail. It should only be mentioned that at the Rayleigh limit, the instability appears if $\Omega < \Omega_A$ for very small Pm and if $\Omega > \Omega_A$ for very large Pm . Both regimes are separated by the Chandrasekhar limit $\Omega = \Omega_A$. The condition $\Omega < \Omega_A$ for very small Pm can be translated into $\text{Re} < \text{Ha}/\sqrt{\text{Pm}}$ which is only true for all Ha if $\text{Pm} \rightarrow 0$. If, for example, a solution exists for

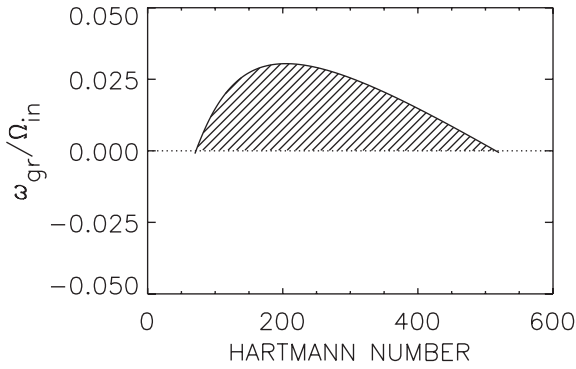


Figure 2. The (normalized) growth rates $\omega_{\text{gr}} = \Im(\omega)/\Omega_{\text{in}}$ as a function of the toroidal background field are only positive in the hatched domain. $m = \pm 1$, $\mu_{\Omega} = 0.25$, $\text{Re} = 3000$, $\text{Pm} = 10^{-6}$.

$\text{Ha} \simeq 100$, then it is immediately clear that the corresponding Re for $\text{Pm} = 10^{-6}$ must be *smaller* than 10^5 .

The meaning of the marginal instability curves is explained by the growth rates, given in Fig. 2 for a fixed Reynolds number $\text{Re} = 3000$. The growth rate is positive between the two critical values, which in Fig. 1 (left-hand panel) enclose a region of instability. The maximum growth rate of 0.02 lies between the two limiting Hartmann numbers, and implies a growth time of about seven rotation times. Compared with the standard MRI, the AMRI is slower, but exhibits the same basic scaling on the rotational time-scale.

As the left-hand plot of Fig. 1 also shows, the AMRI instability domain is always limited by two values of the Reynolds number or two values of the Hartmann number. For a fixed rotation rate, the magnetic field can be too weak or too strong, and conversely for a fixed magnetic field, the rotation can be too slow or too fast.

The azimuthal drift rates (Fig. 1, middle panel) are always negative, hence the pattern of the instability wave drifts in the direction of the basic rotation (see above). A typical value of the drift (normalized with Ω_{in}) for small Pm is 0.25 (marked in the plot), which hardly depends on the Hartmann number. For the rotation ratio $\mu_{\Omega} = 0.25$, the pattern essentially corotates with the outer cylinder. For stronger fields, the drift is slightly slower.

The right-hand plot in Fig. 1 gives the axial wavenumbers normalized with the gap width D . A wavenumber of π (marked) describes a cell with a circular geometry in the radial and the vertical coordinates. Precisely this cell form exists for the instability at the weak-field end of the instability domain. For stronger fields, the cells become more oblate (not prolate!), but this is only true for the lower branches of the instability map. Along the upper branches, the cells preserve their circular shape.

One must ask how the growth rate behaves for increasingly rapid rotation. To answer this question, one must determine the maxima known from Fig. 2 for increasing Reynolds numbers. The results given in Fig. 3 clearly show the saturation of $\omega_{\text{gr}} = \Im(\omega)/\Omega_{\text{in}}$. The maximum growth rate for very rapid rotation is $0.045\Omega_{\text{in}}$, so that the shortest growth time of AMRI at the Rayleigh limit is 3.5 rotation times.

4 QUASI-GALACTIC ROTATION

For the quasi-galactic rotation law with $\mu_{\Omega} = 0.5$, Fig. 4 shows the domain of instability in the S – Rm plane, for various magnetic Prandtl numbers. It is obvious that for $\text{Pm} \lesssim 1$ the values scale with the magnetic Reynolds number Rm and the Lundquist number S .

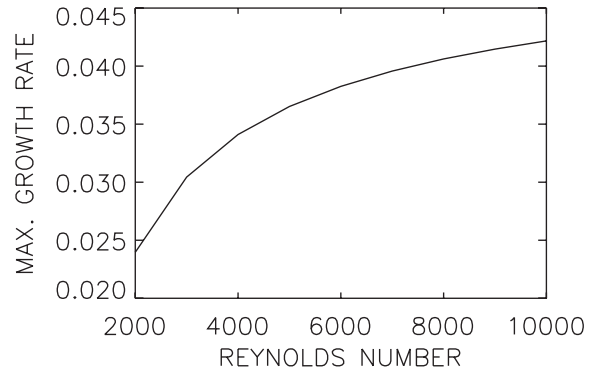


Figure 3. The *maximal* normalized growth rate as a function of the Reynolds number of the basic rotation for $\mu_{\Omega} = 0.25$. The Hartmann numbers which correspond to the maxima vary from about 200 to about 500 from the left-hand to the right-hand axis of the plot. $\text{Pm} = 10^{-6}$.

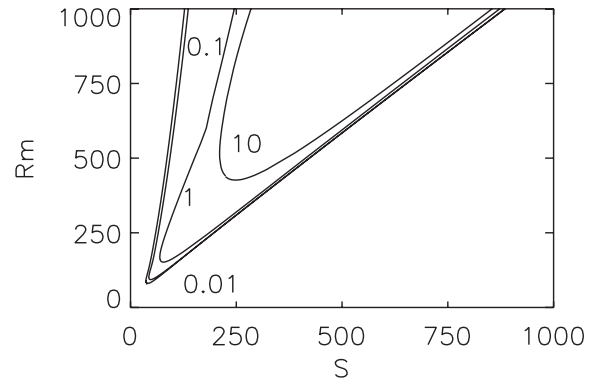


Figure 4. The instability map for the quasi-galactic rotation law $\mu_{\Omega} = 0.5$ in the S – Rm plane. The curves are marked with their values of the magnetic Prandtl number. Curves for $\text{Pm} < 0.01$ are almost identical with the curve for $\text{Pm} = 0.01$. $m = \pm 1$.

The unstable domain in the plane again has the characteristic form of tilted cones, so that minimal and maximal values of both S and Rm always exist for the onset of the instability. Hence, both the magnetic field and the rotation rate can be too weak or too strong for AMRI. One also finds that the instability curves for $\text{Pm} \rightarrow 0$ converge in the S – Rm plane. For all Pm the ratio Ω_{A}/Ω lies between a low-field limit and a high-field limit, e.g. for $\text{Pm} = 1$,

$$0.3 \lesssim \frac{\Omega_{\text{A}}}{\Omega} \lesssim 1. \quad (15)$$

It is thus clear that for AMRI the Alfvén frequency of the toroidal magnetic field and the rotation rate must be of the same order. If the toroidal field is produced by differential rotation acting on a poloidal fossil field, then the low-field limit in equation (15) plays the role of the onset condition for the axisymmetric instability.

For given Rm and Pm , the growth rate has been calculated for $\mu_{\Omega} = 0.5$ between the two limiting values S where it vanishes (see also Fig. 2); it is maximal somewhere between the two limits. In Fig. 5 (bottom panel), the ratio $\omega_{\text{gr}}/\Omega_{\text{in}}$ is plotted for various Rm and for $\text{Pm} = 1$. One finds a quasi-linear relation

$$\frac{\omega_{\text{gr}}}{\Omega_{\text{in}}} \simeq \varepsilon_{\text{gr}} \text{Rm} \quad (16)$$

or

$$\omega_{\text{gr}} \simeq \varepsilon_{\text{gr}} \frac{\Omega_{\text{in}}^2}{\omega_{\eta}} \quad (17)$$

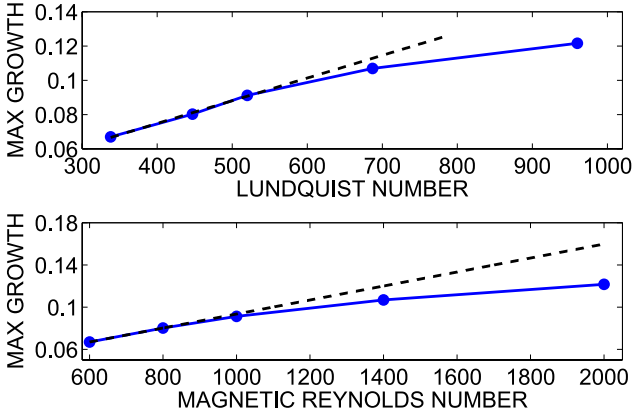


Figure 5. The normalized growth rate $\hat{\omega}_{\text{gr}} = \Im(\omega)/\Omega_{\text{in}}$ and its saturation for $\mu_{\Omega} = 0.5$, optimized in the tilted instability cone for $\text{Pm} = 1$ as a function of S (top panel) or Rm (bottom panel).

with ε_{gr} of the order of 10^{-4} . It varies from 1.5×10^{-4} for $\text{Pm} = 1$ to 2.1×10^{-4} for $\text{Pm} = 0.01$ (not shown), which suggests a very weak dependence of the growth rate ω_{gr} on Pm . Hence, the growth time in units of the rotation time is $\tau_{\text{gr}}/\tau_{\text{rot}} \simeq 10^3/\text{Rm}$ for small Rm . For smaller Rm the AMRI is rather slow, but the linear relation (16) can only hold for small Rm . One also finds that the growth rate slowly grows for smaller Pm , but this effect is rather weak.

The saturation of the normalized growth rates is also demonstrated by Fig. 5. For sufficiently rapid rotation, the dependence of $\hat{\omega}_{\text{gr}}$ on the value of Rm disappears, so that $\Im(\omega)/\Omega_{\text{in}} \leq 0.14$ always holds. The growth time therefore for the instability of the considered rotation law and for $\text{Pm} = 1$ can never be shorter than one rotation time. The same results can also be displayed in terms of the magnetic field (Fig. 5, top panel).

5 AN EXPERIMENT

With the given data, it is easy to design an experiment for the realization of AMRI in the laboratory. For experiments on magnetic-induced instabilities of the differential rotation, it is natural to work with a Taylor–Couette flow between two rotating cylinders and with a rotation law which by itself is hydrodynamically stable. On the other hand, it is reasonable to apply a rotation law very close to the Rayleigh limit, because for small Pm the critical rotation rate scales (only) with Re . Fig. 6 shows that for $\mu_{\Omega} = 0.26$ the limit of

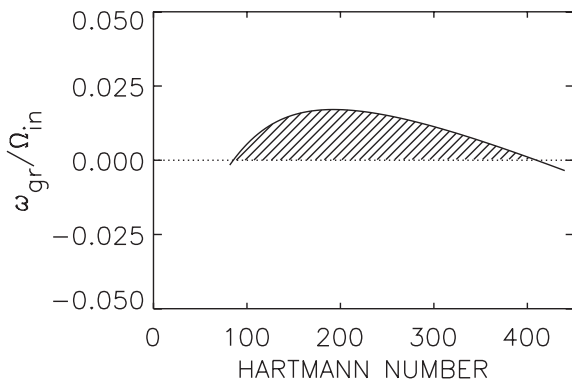


Figure 6. The normalized growth rate for an experiment with $\mu_{\Omega} = 0.26$ as a function of the toroidal background field. $m = \pm 1$; $\text{Re} = 3000$; $\text{Pm} = 10^{-6}$. They are positive only in the hatched domain. There are no visible differences to the results for $\text{Pm} = 0$.

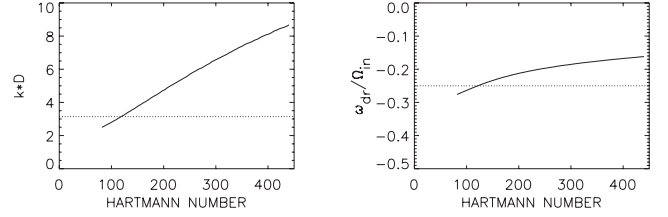


Figure 7. The normalized wavenumber (left-hand panel) and drift rate (right-hand panel) for the fixed Reynolds number $\text{Re} = 3000$. The dotted lines give the wavenumber (π) for a circular cell structure (left-hand panel) and the drift rate of -0.25 for corotation of the pattern with the outer cylinder (right-hand panel). $m = \pm 1$; $\mu_{\Omega} = 0.26$; $\text{Pm} = 10^{-6}$.

marginal instability is reached for a Hartmann number of 85 (and $\text{Re} = 3000$). Note that this instability region is slightly smaller than for the rotation law with $\mu_{\Omega} = 0.25$ (which is understandable as the energy for AMRI is completely provided by the energy of the shear).

The relation $I_{\text{axis}} = 5R_{\text{in}}B_{\text{in}}$ connects the toroidal field amplitude B_{in} at R_{in} with the axial current inside the inner cylinder. I , R and B must be measured in ampere, cm and gauss. Hence,

$$\text{Ha} = \frac{1}{5} \frac{I_{\text{axis}}}{\sqrt{\mu_0 \rho \nu \eta}}. \quad (18)$$

The radial size of the container does not occur in this relation between the Hartmann number and the current amplitude. For the gallium alloy GaInSn, the magnetic Prandtl number is 1.4×10^{-6} and the numerical value of the square root in (18) is 25.6. The resulting electric current for marginal instability is thus 10.9 kA.

For a container with (say) $R_{\text{in}} = 4$ cm, $R_{\text{out}} = 8$ cm and with the viscosity of GaInSn ($\nu = 3.4 \times 10^{-3}$ cm² s⁻¹), the Reynolds number $\text{Re} = 3000$ requires a rotation rate of the inner cylinder of only 0.1 Hz. Fig. 7 shows that for the weakest fields the cell structure of the non-axisymmetric pattern is circular and that the pattern drifts with nearly the same rotation rate as the outer cylinder. Both properties are very characteristic for the instability close to the marginal limit for weak magnetic fields – independent of the steepness μ_{Ω} of the rotation law. Such an experiment is currently operating at the Helmholtz-Zentrum Dresden-Rossendorf. The results will be presented in a separate paper.

6 KINETIC AND MAGNETIC ENERGIES

We have seen that the modes for $m = 1$ and -1 (corresponding to left and right spiralling modes, Hollerbach et al. 2010) are fully degenerate, i.e. they are excited at the same eigenvalues and possess the same wavenumbers and azimuthal phase speeds. To find the resulting instability pattern, non-linear calculations are necessary. For the following calculations, the spectral cylindrical magnetohydrodynamics code of Gellert, Rüdiger & Fournier (2007) is used. The solution is expanded in azimuthal Fourier modes. The resulting meridional problems are solved with a Legendre spectral element method after Deville, Fischer & Mund (2002). The code, however, is only able to solve equations with a minimum magnetic Prandtl number of 0.01. Fig. 8 shows the structure of the resulting wave, which consists of both $m = \pm 1$ components, and drifts together with the outer cylinder. There are seven cells along the vertical axis with its eight length units. The almost circular meridional cell structure thus confirms the results of the linear theory.

Besides the geometric structure, the non-linear code also provides the behaviour of the equilibrated energies. The main question is how

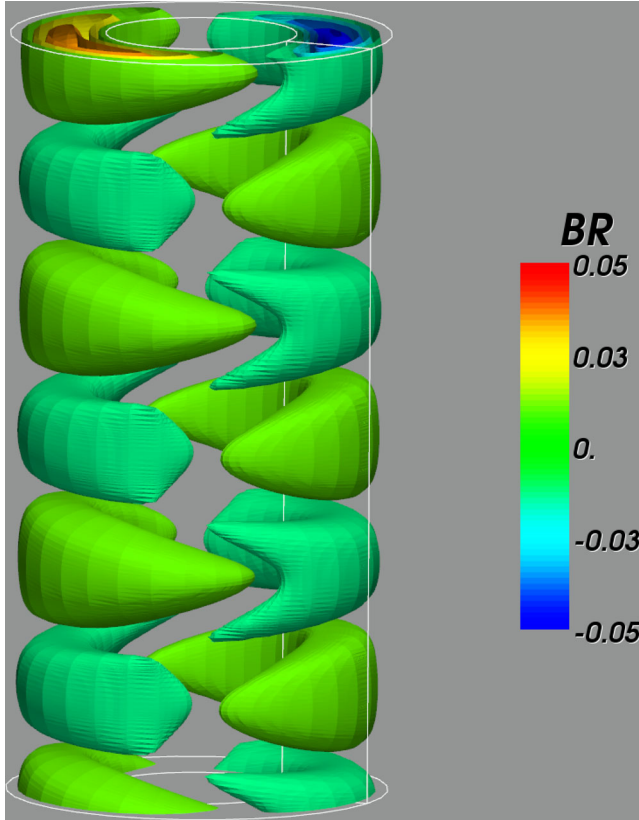


Figure 8. The nonlinear instability pattern of AMRI is a combination of the modes $m = \pm 1$ which drifts with a common drift speed $d\phi/dt$. There are seven cells along the axial direction with the aspect ratio $\Gamma = 8$. The cells are thus slightly elongated. $Re = 500$; $Ha = 80$; $\mu_\Omega = 0.26$; $Pm = 0.1$.

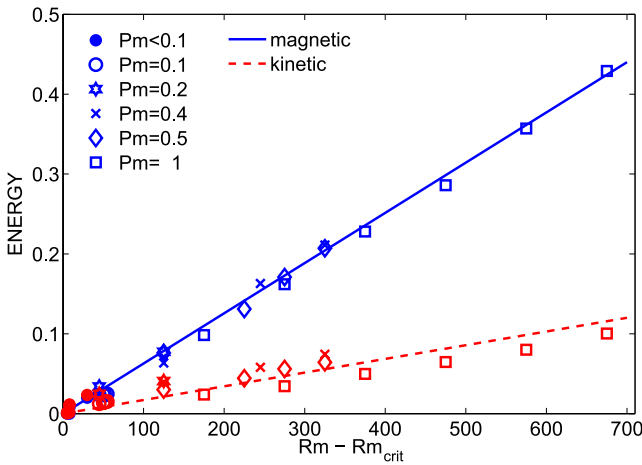


Figure 9. The magnetic (solid line) and the kinetic (dashed line) energies of AMRI for various magnetic Prandtl numbers versus the magnetic Reynolds numbers. $Re = 1000$; $Ha = 75, \dots, 200$; $\mu_\Omega = 0.26$; $Pm = 0.05, \dots, 1$.

strong the magnetic energy is, in units of the kinetic energy. Note that the maximal amplitude of the radial field component in units of B_{in} in Fig. 8 is rather small. This fact, however, is only due to the rather slow rotation of this example.

Fig. 9 displays the energies of several instability realizations for magnetic Prandtl numbers between 0.05 and 1.0. Both the magnetic and the kinetic energy are normalized with the energy of the toroidal background field. All energies are integrals over the entire container.

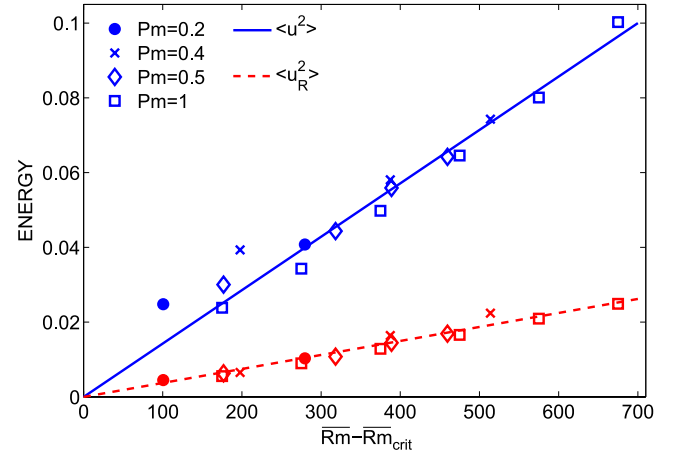


Figure 10. The kinetic energy (solid line) and its portion in the radial direction (dashed line) – both normalized with the energy of the magnetic background field – of the AMRI perturbations for various Pm versus the modified magnetic Reynolds number \overline{Rm} . Note that the radial intensity is almost one-third of the total intensity $\langle u^2 \rangle$. $Ha = 75, \dots, 200$; $\mu_\Omega = 0.26$.

The first finding concerns the quantity $q = \langle b^2 \rangle / B_{in}^2$, which for driven turbulence in the high-conductivity limit scales with Rm (Bräuer & Krause 1974). The same is true for this quantity in the case of AMRI (Fig. 9). The relation

$$q = \varepsilon_{\text{mag}} (Rm - Rm_{\text{crit}}) \quad (19)$$

has been found with $\varepsilon_{\text{mag}} \simeq 6 \times 10^{-4}$. It should thus be possible that the energy of the magnetic fluctuations reaches the order of the magnetic background field. Equation (19) can also be written as $q \propto \varepsilon_{\text{mag}} \Omega / \omega_\eta$. The saturation of q for large magnetic Reynolds numbers, however, is not yet known. A possible form of the relation for fast rotation might be $q \propto \Omega_A^2 / \Omega^2$.

Fig. 9 also shows that the magnetic energy always dominates the kinetic energy of the fluctuations. One may speculate that the factor of 4 which arises here also appears in the ratio of the resulting eddy viscosity and the chemical diffusivity (see below).

According to Fig. 10 the kinetic energy for various magnetic Prandtl numbers versus the modified Reynolds number $\overline{Rm} = \Omega_{in} R_{in}^2 / \bar{\eta}$ with $\bar{\eta} = \sqrt{\nu \eta}$ provides the linear relation

$$\frac{\mu_0 \rho \langle u^2 \rangle}{B_{in}^2} = \varepsilon_{\text{kin}} (\overline{Rm} - \overline{Rm}_{\text{crit}}) \quad (20)$$

with $\varepsilon_{\text{kin}} \simeq 1.4 \times 10^{-4}$. Hence,

$$\frac{u_{\text{rms}}}{\Omega_{in} R_{in}} \simeq 0.012 \bar{\Lambda}^{0.5} \quad (21)$$

with the modified Elsasser number

$$\bar{\Lambda} = \frac{B_{in}^2}{\mu_0 \rho \Omega \bar{\eta}}, \quad (22)$$

which again does *not* depend on the size of the container. The appearance of the molecular viscosity in the expression of the kinetic energy might have strong consequences for the value of the kinetic energy. For not too small Pm , however, it is clear that the AMRI provides higher values of the magnetic energy compared with the kinetic energy. This means that the resulting eddy viscosity also exceeds the mixing coefficient of chemicals. The angular momentum transport is dominated by the magnetic energy, while magnetic fluctuations do not contribute to the diffusion of thermal energy and/or the mixing of chemicals (Vainshtein & Kichatinov 1983).

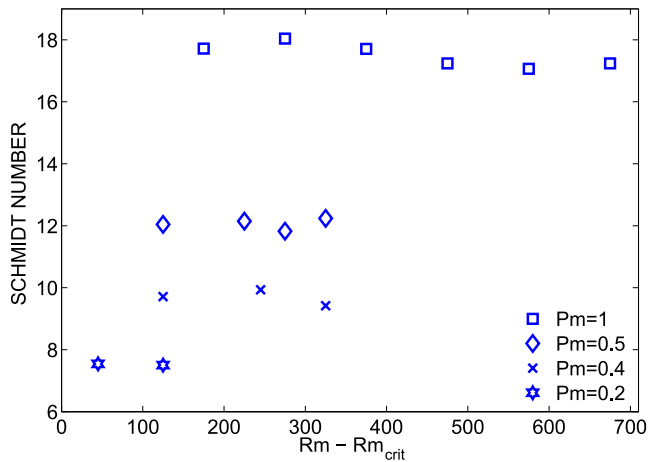


Figure 11. The proxy (24) of the turbulent Schmidt number for various magnetic Prandtl numbers and for $\mu_\Omega = 0.26$ does *not* depend on the magnetic Reynolds number but decreases as \sqrt{Pm} .

The different scaling of the magnetic and kinetic energies has consequences for their ratio $\epsilon = \langle \mathbf{b}^2 \rangle / \mu_0 \rho \langle \mathbf{u}^2 \rangle$, which after (19) and (20) scales as \sqrt{Pm} . The magnetic energy only dominates for magnetic Prandtl numbers of the order of unity or larger. Consequently, the turbulent Schmidt number

$$Sc = \frac{\nu_T}{D_T} \simeq \epsilon_R \quad (23)$$

should also scale with \sqrt{Pm} . Here ϵ_R is formed with the radial velocity components (also given in Fig. 10), i.e.

$$\epsilon_R = \frac{\langle \mathbf{b}^2 \rangle}{\mu_0 \rho \langle u_R^2 \rangle}, \quad (24)$$

as only the radial turbulent intensity is responsible for the radial mixing of chemicals. Fig. 11 demonstrates that indeed the turbulent Schmidt number on the basis of AMRI strongly exceeds unity, but decreases with \sqrt{Pm} for small Pm. There is no clear evidence for a strong dependence of the Schmidt number on the basic rotation. Note, however, that for very small magnetic Prandtl numbers, it cannot become smaller than 0.4 (Yousef, Brandenburg & Rüdiger 2003). In fluids with a small magnetic Prandtl number, the angular momentum transport and the mixing of chemicals by AMRI are of the same power. Both processes stop when rigid rotation is reached.

Only as long as the differential rotation is strong the mixing of chemicals is strong. It might be, however, that the inclusion of the ‘negative’ buoyancy by the stable stratification of real stellar cores only reduces the mixing rather than the angular momentum transport, and the Schmidt number is not reduced too much by the small magnetic Prandtl number (Kitchatinov & Brandenburg 2012).

ACKNOWLEDGEMENTS

This work was supported by the Deutsche Forschungsgemeinschaft (SPP 1488 *PlanetMag*). RH is supported at ETH Zürich by ERC Grant No. 247303 (MFECE).

REFERENCES

- Bräuer H. J., Krause F., 1974, *Astron. Nachr.*, 295, 223
 Chandrasekhar S., 1956, *Proc. Natl. Acad. Sci. USA*, 42, 273
 Deville M. O., Fischer P. F., Mund E. H., 2002, *High-Order Methods for Incompressible Fluid Flow*. Cambridge Univ. Press
 Eggenberger P., Montalbán J., Miglio A., 2012, *A&A*, 544, L4
 Gellert M., Rüdiger G., Fournier A., 2007, *Astron. Nachr.*, 328, 1162
 Hollerbach R., Teeluck V., Rüdiger G., 2010, *Phys. Rev. Lett.*, 104, 44502
 Kirillov O. N., Stefani F., Fukumoto Y., 2012, *ApJ*, 756, 83
 Kitchatinov L. L., Brandenburg A., 2012, *Astron. Nachr.*, 333, 230
 Kitchatinov L. L., Rüdiger G., 2010, *A&A*, 513, L1
 Michael D. H., 1954, *Mathematika*, 1, 45
 Rüdiger G., Hollerbach R., 2004, *The Magnetic Universe*. Wiley-VCH
 Rüdiger G., Kitchatinov L. L., 1996, *ApJ*, 466, 1078
 Rüdiger G., Hollerbach R., Schultz M., Elstner D., 2007, *MNRAS*, 377, 1481
 Rüdiger G., Gellert M., Schultz M., Strassmeier K. G., Stefani F., Gundrum T., Seilmayer M., Gerbeth G., 2012, *ApJ*, 755, 181
 Seilmayer M., Stefani F., Gundrum T., Weier T., Gerbeth G., Gellert M., Rüdiger G., 2012, *Phys. Rev. Lett.*, 108, 244501
 Stefani F., Gerbeth G., Gundrum T., Hollerbach R., Priede J., Rüdiger G., Szklarski J., 2009, *Phys. Rev. E*, 80, 066303
 Tayler R. J., 1957, *Proc. Phys. Soc., Section B*, 70, 31
 Tayler R. J., 1973, *MNRAS*, 161, 365
 Vainshtein S. I., Kichatinov L. L., 1983, *Geophys. Astrophys. Fluid Dyn.*, 24, 273
 Vandakurov Y. V., 1972, *SvA*, 16, 265
 Velikhov E. P., 1959, *Sov. Phys. JETP*, 9, 995
 Yousef T. A., Brandenburg A., Rüdiger G., 2003, *A&A*, 411, 321

This paper has been typeset from a $\text{\TeX}/\text{\LaTeX}$ file prepared by the author.